AIP | Applied Physics Letters

Optofluidic Fabry–Pérot cavity biosensor with integrated flow-through micro-/nanochannels

Yunbo Guo, Hao Li, Karthik Reddy, Hrishikesh S. Shelar, Vasuki R. Nittoor et al.

Citation: Appl. Phys. Lett. **98**, 041104 (2011); doi: 10.1063/1.3548673
View online: http://dx.doi.org/10.1063/1.3548673
View Table of Contents: http://apl.aip.org/resource/1/APPLAB/v98/i4
Published by the AIP Publishing LLC.

Optofluidic Fabry–Pérot cavity biosensor with integrated flow-through micro-/nanochannels

Yunbo Guo, Hao Li, Karthik Reddy, Hrishikesh S. Shelar, Vasuki R. Nittoor, and Xudong Fan[a)]
Department of Biomedical Engineering, University of Michigan, Ann Arbor, 1101 Beal Ave., Ann Arbor, Michigan 48109-2110, USA

(Received 16 December 2010; accepted 6 January 2011; published online 24 January 2011)

An optofluidic Fabry–Pérot cavity label-free biosensor with integrated flow-through micro-/nanochannels is proposed and demonstrated, which takes advantages of the large surface-to-volume ratio for analyte concentration and high detection sensitivity and built-in fluidic channels for rapid analyte delivery. The operating principle is first discussed, followed by assembly of a robust sensing system. Real-time measurements are performed to test its sensing feasibility and capability including bulk solvent change and removal/binding of molecules from/onto the internal surface of fluidic channels. The results show that this sensor provides a very promising platform for rapid, sensitive, and high-throughput biological and chemical sensing. © *2011 American Institute of Physics*. [doi:10.1063/1.3548673]

Label-free sensors enable the detection of chemical and biological samples in their natural forms without external fluorescence labeling and therefore are of great interest in healthcare, biochemical research, and homeland security.[1] Effective integration between label-free sensors and microfluidics is highly desirable for efficient sample delivery to achieve rapid and sensitive detection. To date, most of the label-free sensors employ the "flow-over" scheme, which relies on the analytes in bulk solution to diffuse to the sensing surface. While simple, this approach suffers from mass transport problems that significantly slow down the detection speed, particularly at low sample concentrations. Recently, the "flow-through" scheme has been implemented in a few label-free sensors.[2–6] In those designs, an array of nanoholes is created on a thin (~100 nm) dielectric or metallic membrane to form photonic crystals or nanoplasmonic structures for sensing, as well as nanofluidic channels for analytes to flow through. Using this method, 6–14-fold improvement in the mass transport rate has been demonstrated.[3,4] However, fabrication of those nanostructures is very costly and involves many steps. Furthermore, it is challenging or laborious to ensure the structural integrity of the membranes, which is subject to relatively high pressure gradients required to drive analytes through. Additionally, the Q-factors in those sensors are still low (~10–30),[2–4] adversely affecting their sensing performance. Finally, since the hole size determines the sensor operation wavelength, there is little design flexibility in selecting holes to accommodate different sizes of analytes that range from protein molecules (~5–10 nm) to viral particles (hundreds of nanometers).

In this letter, we propose, fabricate, characterize, and demonstrate an optofluidic Fabry–Pérot (FP) cavity sensor with integrated flow-through micro-/nanofluidic channels. As illustrated in Fig. 1(a), the optofluidic FP sensor employs a microsized capillary with many built-in micro-/nanosized flow-through holes. When the capillary is placed between two reflectors, a FP cavity forms and detects the analytes that bind to the internal surface of the holes. The optofluidic FP sensor has a number of advantages over the current label-free sensors. First, as opposed to the planar surface detection in most sensors, micro-/nanohole arrays enable three-dimensional detection, which greatly enhances the detection sensitivity. Our sensor mimics the nanoporous silicon sensor with high sensitivity,[7–10] and meanwhile significantly expedites the detection speed (minutes versus hours[8,9]) due to its built-in flow-through fluidics (rather than dead-ended holes in the nanoporous silicon sensor). Second, the micro-/nanofluidic capillary can be mass-produced easily and cost-effectively from a preform using the fiber drawing method with a much narrower hole size distribution than the nanoporous silicon sensor. It is highly robust and can sustain relatively high pressure. Third, the hole size can be adjusted to accommodate a wide range of biological samples without significantly altering the setup or operation wavelength. Fi-

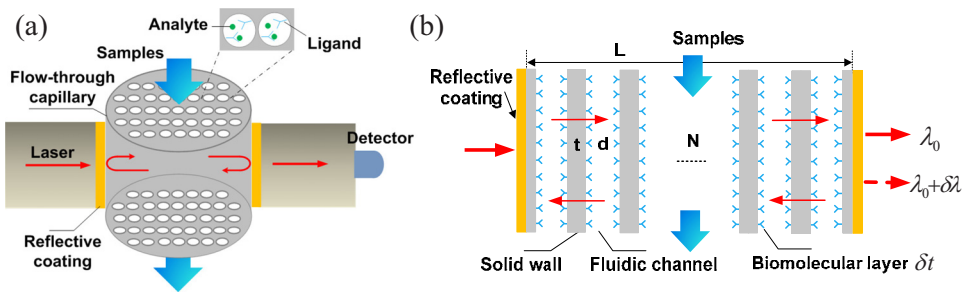

FIG. 1. (Color online) (a) Illustration of the FP sensor with integrated flow-through micro-/nanofluidic channels. (b) Illustration of the one-dimensional FP sensor. Resonance wavelength undergoes a spectral shift ($\delta\lambda$) when biomolecules bind to the sensor inner surface.

[a)]Electronic mail: xsfan@umich.edu.

nally, the Q-factor of the FP resonator can be as high as 27 000,[11] about three orders of magnitude higher than the aforementioned flow-through sensors, which, together with the higher sensitivity, should lead to a much better sensing performance.

Figure 1(b) illustrates the optofluidic FP sensing principle using a simple one-dimensional FP cavity composed of N holes, which provides $2N$ solid-liquid interfaces for biomolecular adsorption. The initial resonance wavelength λ_0 is determined by the resonant condition: $2nL=m\lambda_0$ $(m=1,2,3,\ldots)$, where n and L are the effective refractive index (RI) and length of the cavity, respectively. After biomolecule attachment, the resonant condition becomes $2(nL+2N\cdot\Delta n\cdot\delta t)=m(\lambda_0+\delta\lambda)$, where Δn is the RI difference between the biomolecule and the ambient medium within the fluidic channels (e.g., water), δt is the thickness of the adsorbed biomolecular layer, and $\delta\lambda$ is the resonant wavelength shift. Therefore, the surface detection sensitivity, $\delta\lambda/\delta t$, is given by $\delta\lambda/\delta t=2N(\Delta n/nL\cdot\lambda_0)$, $2N$-fold enhancement over the FP cavity sensor with a single sensing surface.[12]

A more generalized expression for the surface detection sensitivity can be deduced by considering the mode spectral shift caused by the fractional electromagnetic energy change inside the cavity due to the biomolecular attachment,[13,14]

$$\delta\lambda/\delta t=(A/V)(\Delta n/n)\lambda_0, \tag{1}$$

where V and A are the total volume and internal surface area within the FP cavity, respectively. Equation (1) shows that the surface detection sensitivity is linearly proportional to the surface-to-volume ratio, A/V. Similarly, the bulk refractive index sensitivity (assuming that the RI of all fluidic channels is homogeneously changed), $\delta\lambda/\delta n$, can be derived as

$$\delta\lambda/\delta n=(W/V)(\lambda_0/n), \tag{2}$$

where W is the total volume of the fluidic channels within the FP cavity. The bulk RI sensitivity can be used to characterize the capability of detecting large species (such as virus).

Figure 2 plots the simulation results based on Eq. (1) for a FP cavity with square holes. With the decreased hole size, more holes and hence more surface area can be placed inside the cavity, resulting in a larger surface detection sensitivity. For the hole size from 1 μm to 20 nm, a sensitivity of 0.47–23 nm/nm can be achieved. The sensitivity for the 20–100 nm holes is on par with the nanoporous silicon sensor with the similar pore sizes,[10] but much larger than nearly all other types of label-free sensors such as surface plasmon resonance sensors, photonic crystal sensors, and ring resonator sensors.[1]

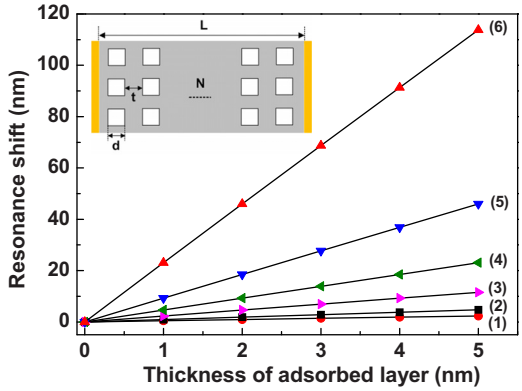

FIG. 2. (Color online) Simulation of the sensor's spectral shift as a function of the adsorbed layer thickness for different hole sizes based on Eq. (1). Holes are square and the wall thickness t is the same as the hole size d. $d=1$, 0.5, 0.2, 0.1, 0.05, 0.02 μm for curves (1)–(6). $\lambda_0=1550$ nm, $\Delta n=0.2$, $L=100$ μm. The inset illustrates the hole arrangement.

In the proof-of-concept experiments, we first fabricate micro-/nanofluidic capillaries [as exemplified in Figs. 3(a) and 3(b)] using an in-house computer controlled fiber/capillary drawing system and a borosilicate glass preform having 7000 uniform 18 μm hexagonal holes. Figure 3(c) shows the experimental setup. A piece of 6-mm-long capillary [shown in Fig. 3(a)] is placed between two gold coated single mode fibers. The light from a tunable laser (1520–1570 nm) is coupled into one fiber and the transmitted light is collected by the other one. One end of the capillary is connected to a sample reservoir, and the sample is withdrawn by vacuum from the other end with a flow rate of $\sim$0.5 μL/min.

Figure 4(a) shows the transmission spectra of the FP cavity in the absence and presence of the capillary [filled with de-ionized (DI) water]. The presence of the capillary increases the cavity optical length, thus resulting in a smaller free spectral range. Note that even with thousands of holes inside the cavity, the FP resonance still persists with a full width at half maximum of about 3.1 nm (obtained by Lorentz fitting), corresponding to a Q-factor of 500 (much higher than other flow-through sensors[2–4]). The Q-factor can significantly be improved in the future by using a collimated beam instead of the diverging beam from the fiber[15] and highly reflective dielectric multilayers instead of the lossy gold film.[11,12] Note that the resonances observed in Fig. 4(a) are not due to the photonic band gap effect resulting from the orderly arranged holes.[16] Randomly distributed holes should work just well, like in a nanoporous silicon sensor.

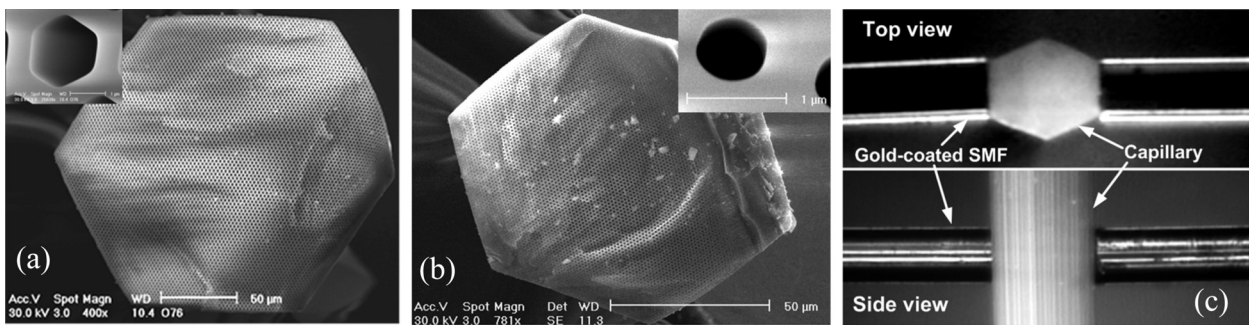

FIG. 3. [(a) and (b)] Scanning electron microscopy (SEM) images of a 200 μm capillary with 1.80 μm holes and a 90 μm capillary with 650 nm holes. The insets show the enlarged images of the holes. (c) Pictures of the experimental setup.

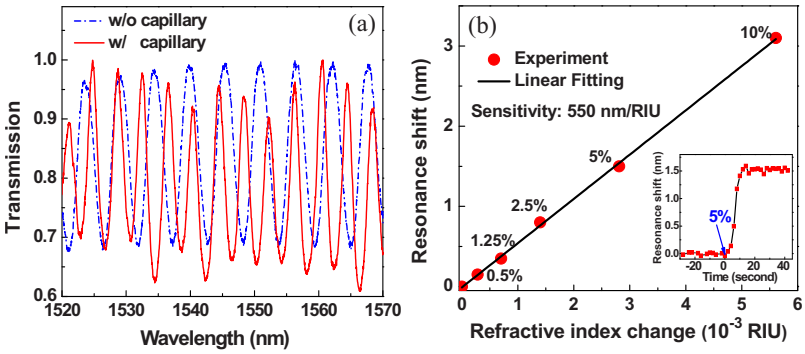

FIG. 4. (Color online) (a) Normalized transmission spectra of the FP cavity in the absence/presence of the capillary. (b) Characterization of the sensor's bulk RI sensitivity. The inset shows the sensorgram for 5% ethanol flowing through the capillary to replace DI water.

We then characterize our sensor's bulk RI detection capability by flowing a series of ethanol and DI water mixtures. Figure 4(b) shows that 550 nm/RIU (refractive index units) can be obtained, close to our theoretical estimation of 640 nm/RIU using Eq. (2). This sensitivity is similar to that achieved in other flow-through sensors.[2,3] As shown in the inset of Fig. 4(b), it takes less than 15 s for 5% ethanol to completely replace the DI water initially filled inside the capillary. This represents the quickest analyte delivery rate among all flow-through nanohole sensors, as our sensor does not require any external microfluidic channels to be connected to the nanoholes.

To characterize the surface detection capability of our sensor, in Fig. 5(a) we employ silica molecule as the low molecular weight (MW) model system (MW=60 Da) and monitor the sensor response when silica molecules are continuously removed from the wall when low concentration (1%) aqueous hydrofluoric acid (HF) is flowed through the capillary. A total blueshift of 3.7 nm within 1.7 min is observed. Independent experiment shows that the etching rate of 1% HF for borosilicate glass is 20 nm/min. Therefore, the sensor surface detection sensitivity is approximately 0.109 nm/nm, close to the theoretical estimation of 0.124 nm/nm based on Eq. (1).

In addition to detecting molecules removed from the sensing surface, we also measure the biomolecules attached to the surface. First, the internal surface of the capillary is activated by 1% HF etching, followed by 5% aminopropyltrimethoxysilane solution in methanol/DI water (1:1). Then phosphate buffered saline (PBS) buffer is flowed continually to remove the residual solution and establish a stable baseline. At time zero, 1 mg/ml EZ-Link® sulfo-NHS-LC-LC-biotin (sulfosuccinimidyl-6-[biotinamido]-6-hexanamido hexanoate) (MW=670 Da) in PBS is flowed into the capillary. Figure 5(b) shows that the wavelength shift increases as more analytes covalently bind to the sensing surface until a saturation shift of 0.35 nm is reached in about 7 min. No blueshift is observed with the subsequent PBS rinse, indicating that analytes are strongly bound to the sensor surface. Assuming that a fully packed analyte layer is formed on the sensing surface with the thickness increase corresponding to the length of analyte (i.e., 3.05 nm) and that the analyte has the same RI as silica, we arrived at the surface detection sensitivity of 0.115 nm/nm, close to 0.124 nm/nm based on Eq. (1) discussed earlier.

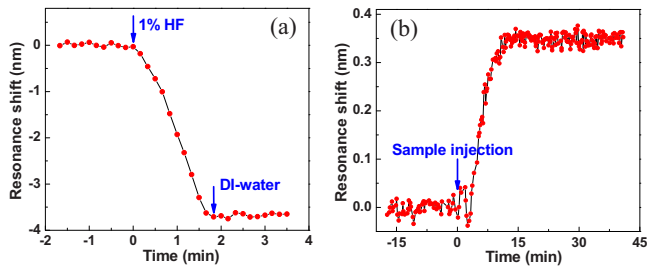

FIG. 5. (Color online) (a) Sensorgram when silica molecules on the sensor wall are removed by 1% HF. (b) Sensorgram of 1 mg/ml sulfo-NHS-LC-LC-biotin binding to the silanized silica sensing surfaces inside the capillary.

In conclusion, we have presented a robust optofluidic FP cavity sensor with integrated flow-through micro-/nanochannels, which exhibits rapid analyte delivery, high bulk RI sensitivity, and potentially high surface detection sensitivity. In the future, we will improve the Q-factor by using highly reflective dielectric multilayers. The surface detection sensitivity will also be increased by using smaller holes and higher hole density. A shorter capillary (<1 mm) will be employed for even quicker sample delivery.

[1]X. Fan, I. M. White, S. I. Shopova, H. Zhu, J. D. Suter, and Y. Sun, Anal. Chim. Acta **620**, 8 (2008).
[2]M. Huang, A. A. Yanik, T. Chang, and H. Altug, Opt. Express **17**, 24224 (2009).
[3]A. A. Yanik, M. Huang, A. Artar, T. Chang, and H. Altug, Appl. Phys. Lett. **96**, 021101 (2010).
[4]F. Eftekhari, C. Escobedo, J. Ferreira, X. Duan, E. M. Girotto, A. G. Brolo, R. Gordon, and D. Sinton, Anal. Chem. **81**, 4308 (2009).
[5]D. Sinton, R. Gordon, and A. G. Brolo, Microfluid. Nanofluid. **4**, 107 (2008).
[6]C. Escobedo, A. G. Brolo, R. Gordon, and D. Sinton, Anal. Chem. **82**, 10015 (2010).
[7]V. S. Y. Lin, K. Motesharei, K. S. Dancil, M. J. Sailor, and M. R. Ghadiri, Science **278**, 840 (1997).
[8]M. M. Orosco, C. Pacholski, and M. J. Sailor, Nat. Nanotechnol. **4**, 255 (2009).
[9]S. Chan, P. M. Fauchet, Y. Li, L. J. Rothberg, and B. L. Miller, Phys. Status Solidi A **182**, 541 (2000).
[10]H. Ouyang, C. C. Striemer, and P. M. Fauchet, Appl. Phys. Lett. **88**, 163108 (2006).
[11]M. W. Pruessner, T. H. Stievater, and W. S. Rabinovich, Opt. Lett. **32**, 533 (2007).
[12]D. A. Bergstein, E. Ozkumur, A. C. Wu, A. Yalcin, J. R. Colson, J. W. Needham, R. J. Irani, J. M. Gershoni, B. B. Goldberg, C. DeLisi, M. F. Ruane, and M. S. Ünlü, IEEE J. Sel. Top. Quantum Electron. **14**, 131 (2008).
[13]S. Arnold, M. Khoshsima, I. Teraoka, S. Holler, and F. Vollmer, Opt. Lett. **28**, 272 (2003).
[14]S. Arnold, R. Ramjit, D. Keng, V. Kolchenko, and I. Teraoka, Faraday Discuss. **137**, 65 (2008).
[15]Y. Jiang and C. Tang, Smart Mater. Struct. **17**, 055013 (2008).
[16]P. Domachuk, H. C. Nguyen, B. J. Eggleton, M. Straub, and M. Gu, Appl. Phys. Lett. **84**, 1838 (2004).